AIAA

Colliding Stellar Winds in the Eclipsing Wolf-Rayet Binary V444 Cygni

DOUGLAS N. BROWN[1,4] and STEVEN N. SHORE [2,3,4]

Received:————; *Accepted:*————.

1. Department of Astronomy, University of Washington

2. Astrophysics Research Center, Department of Physics, New Mexico Institute of Mining and Technology

3. DEMIRM, Observatoire de Meudon

4. Guest Investigator, *International Ultraviolet Explorer* Satellite

Submitted to Ap.J.

ABSTRACT .

We have obtained high resolution spectra of V444 Cygni with the *International Ultraviolet Explorer* Satellite. These spectra span both eclipses and include one observation at third quadrature. Together with seven archival spectra, they provide reasonably complete phase coverage for the system. The variations in the P Cygni profiles of the He II and N IV lines imply the existence of a low density region in the WR wind. This region occupies a relatively narrow range of orbital phase coinciding with the highest terminal velocities observed in C IV. We interpret these data as evidence of an interaction region separating the winds of the O-star and Wolf-Rayet star.

GODDARD
NAG5-537
IN-90-CR
146705
218

I. Introduction

The importance of the Wolf-Rayet binary V444 Cygni = HD 193576 (O6-8 III:+ WN4 AB; Walborn 1974) is that the system affords an almost unique laboratory for studying the structure of a massive radiatively driven stellar wind. In consequence of the atmospheric eclipse of the primary by the Wolf-Rayet (WR) secondary, the density and velocity structures of the constituent stellar winds are encoded in the variation of ultraviolet line profiles with orbital phase. V444 Cygni is the only eclipsing WR + O binary which is bright enough to be conveniently studied at high resolution with the *International Ultraviolet Explorer* (IUE).

Radial velocity studies (Wilson,1940,1942; Keeping,1947; Münch,1950) have established the orbital parameters: $a = 40R_\odot$, $M_{O6} = 25M_\odot$, and $M_{WN} = 10M_\odot$. The most recent photometric solution (Cherepashchuk and Khaliullin 1973; Cherepashchuk, Eaton, and Khaliullin 1984, hereafter CEK), based on analysis of the eclipses at wavelengths between 2460 Å and 3.5μ, yields the orbital inclination, $i = 78°$, radius of the primary, $R_{O6} = 10R_\odot$; and the radius of the WR core, $R_{WN} = 2.9R_\odot$. These values are consistent with earlier photometric determinations (Kron and Gordon 1943, 1950) and with a polarimetric determination of the orbital inclination by Rudy and Kemp (1978).

The unequal durations of primary and secondary eclipse have generally been considered to imply that the WR core is surrounded by an extended, optically thin, strongly limb-darkened outer atmosphere (Kopal, 1944) of radius roughly three times that of the core (Russell, 1944). Kopal and Shapley (1946) predicted that electron scattering was the principal source of continuous opacity in this dilute envelope, a fact confirmed by the observation that the shape of primary eclipse is independent of the wavelength of observation (Hiltner, 1949).

The mass loss rate has been determined by two methods. Bieging, *et al.* (1982) and Abbott, *et al.* (1986) have measured the free-free emission at 4885 MHz. and derived $\dot{M} = 1.4 \times 10^{-5} M_\odot yr^{-1}$ on the basis of the theory of Wright and Barlow (1975). Khaliullin (1974) and Kornilov and Cherepashchuk (1979) have used the rate of change of the orbital period (see eq. 1) and the assumption of radial outflow from the WR component to infer $\dot{M} = 1.2 \times 10^{-5} M_\odot yr^{-1}$.

CEK find that the color temperature of the WR core in the optical-ultraviolet range is approximately 20,000 K, while the electron temperature is 80,000 - 100,000 K. The wide wavelength range of their data allowed CEK to determine the run of the volume extinction coefficient with radial distance from the WR component. Attributing the extinction to Thompson scattering and assuming that the electrons arise entirely from the double ionization of helium, they determined that at the WR core, $n_e = 9 \times 10^{12} cm^{-3}$ and v = 400 kms^{-1}. They find that the wind velocity increases steeply, attaining an outflow velocity near 2000 kms^{-1} at $r = 10R_\odot$. The wind accelerates more gradually at larger radii, attaining its terminal velocity (2500 kms^{-1}) at a distance of 20 to 30 $R_\odot$.

The optical spectrum is dominated by high excitation emission lines of He II, N III, N IV and N V which display a strikingly diverse range of phase dependent variations (Munch, 1950). The blend of He II and N III at λ4542 is stronger at primary eclipse than at secondary and weakest at elongations, while N III λ4640 is stronger at secondary minimum than at primary. The flux in the N III λ3483 emission feature is roughly independent of orbital phase except at primary eclipse, when the emission weakens markedly and a strong absorption feature appears. In contrast, N IV λ4058 lacks absorption at any phase and is strongest at primary minimum.

Kuhi (1968a) obtained narrow-band light curves through secondary eclipse in

the principal optical emission lines. His results confirm the diversity of line variations (some lines do not show eclipses at all) and also reveal the magnitude of intrinsic intensity fluctuations in the optical emission lines. Flux differences at constant phase of order tens of percent were found, even when the observations were separated by only a few orbital periods. Kuhi determined from his observations that the WR atmosphere, though optically thin in the continuum, is optically thick in the emission lines and suggested that electron scattering of line radiation contributes significantly to the (fluctuating) characteristics of the narrow band eclipse curves. He was accordingly unable to account for his light curves on the basis of geometrical considerations alone. From the general tendency for emission lines to be weaker at primary than at secondary eclipse, he inferred that a significant fraction of the flux emitted in lines comes from a small cylindrical region between the two stars.

Kuhi (1968b) and Bisiacchi, et al. (1982) found that the profile of He II λ4686 is symmetrical at both elongations but asymmetrical to opposite sides during primary and secondary eclipse; it is shaded to the blue at primary eclipse and shaded to the red at secondary. Sahade (1958) reported the detection of a narrow emission component superimposed on the broad λ4686 emission feature. He interprets the radial velocity variations of this component as indicative of an origin near the Lagrangian point, L_1 of the system. Underhill (1966) has suggested that the presence of sharp displaced absorption features particularly near primary eclipse ($\Phi = 0.^p00$) is evidence for gas streaming in the system.

Recently, low dispersion IUE spectra have been employed to characterize the variations of UV emission lines in this system. Eaton, Cherepashchuk and Khaliullin (1985, hereafter ECK) noted that the C IV $\lambda\lambda$1548, 1550 and Si IV $\lambda\lambda$1396, 1403 resonance doublets showed P Cygni profiles with the largest terminal velocities and least

dependence on orbital phase, while the N IV λ1718 subordinate line showed the lowest terminal velocity and greatest phase dependence. Additionally, they noted that the He II λ1640 and N IV λ1718 lines showed weak absorption components near secondary eclipse. Synthetic photometry in these lines showed:

1. Primary flux minimum for He II, N IV, and Si IV are displaced from the continuum mid-eclipse phase, occurring at $\Phi = 0.05$.

2. In He II and N IV, the flux increases between phases 0.25 and 0.45.

3. The emission in all three of these lines decreases at secondary eclipse.

They interpret these light curves in terms of a model in which the emitting region lies within $9 \pm 4R_\odot$ of the WR component but the absorption arises in a spherical shell of inner radius $\approx 10R_\odot$ and outer radius external to the system. The brightening of λ1640 and λ1718 between $\Phi = 0.25$ and $\Phi = 0.45$ ($\approx$ 5 percent of the continuum flux) is interpreted as a binary reflection effect: the O star radiation reflected off the expanding WR envelope. In contrast, light curves in the N IV] λ1486, C IV $\lambda\lambda$1548,50 and N V λ1240 display little if any phase dependence, whereby ECK infer that they are formed exterior to the formation region of the He II and N IV lines.

Koenigsberger and Auer (1985) measured fluxes and equivalent widths in emission and absorption components of some P Cygni lines as well as velocities of identifiable points on the line profiles. They determined that both the emission and absorption components of He II λ1640 and N IV λ1718 profiles vary with phase. Most striking was their observation that the blue-shifted absorption of C IV λ1550 is narrower at primary eclipse than near secondary eclipse. They attributed this difference to the contribution of an O-star wind which reaches a higher terminal velocity than that of the WR wind. Accordingly, they suggested the likelihood of a wind-wind interaction region between the two stars.

Favoring an alternative viewpoint, Underhill (1983a,b;1984 a,b;1986) has persistently criticised the widely accepted notion that WR stars possess relatively small hot cores and powerful, radiatively driven winds. Underhill and Fahey (1987) argue that, because of the presence of weak unresolved emission lines, the UV light curves derived (as those of ECK) from low resolution IUE spectra do not represent true continuum fluxes. They derive continuum fluxes from a series of 13 high-resolution IUE spectra of V444 Cygni. Comparing these data with the optical light curves of CEK, they argue for the presence of sufficient phase dependent "third light" shortward of 1500 Å to invalidate the light curve analysis of Cherepashchuk and his collaborators. On the basis of the orbital phase dependent variations of the He II λ1640 profile, they recommend a model in which the WR component has $T_{eff} = 30{,}000$ K, $R = 9R\odot$ and possesses large magnetically-supported plumes which contribute much of the optical and UV line emission.

The original goal of the observations reported here was to determine the density and velocity structure of the WR wind directly from the absorption components of the ultraviolet P Cygni profiles. By subdividing the WR wind absorption profiles through secondary eclipse into bins of ~ 300 km s^{-1}, we planned to generate a set of light curves, each specific to a single projected expansion velocity. We would thus obtain the total optical depth along iso-velocity surfaces for each impact parameter. In principle it is possible to obtain, from the phase dependence of this optical depth, both the density and velocity structure of the WR wind. In practice, the intended Doppler tomography was incompletely realized because O-star absorption profile is not separable in the IUE spectra, even at quadrature when the velocity difference between the components is greatest. Nevertheless, the spectra obtained for this program reveal very important features of the binary system.

II. Observations

The new observations discussed here were obtained using the SWP camera of the IUE satellite during low noise (US1) shifts in 1985 May/June. The large aperture was used for maximum throughput and because of the uncertain flux calibration of small aperture high resolution spectra. The choice of exposure times was determined by the need to achieve maximum phase resolution consistent with acceptable S/N at C IV λ1550. Because the star is relatively faint and heavily reddened, the longest exposure which could be accommodated in a half-shift yielded S/N in the continuum at λ1550 of roughly 5:1, only half that expected for an optimal exposure. These spectra were supplemented by those archival images which were taken through the large aperture and which have acceptable noise levels. Several archival images were rejected because of poor S/N, although their omission left phase gaps. A journal of the new observations is presented in Table 1, while corresponding data for the archival spectra appears in Table 2.

The spectra are phased according to the ephemeris of Kornilov and Cherepashchuk (1979)

$$HJD(primaryeclipse) = 2441164.337 + 4.^d212435(E) \qquad (1)$$

supplemented by a correction for the observed rate of period change (Cherepashchuk 1982). For SWP 14553, (O-C) = $-0.^p011$, while (O - C) = $-0.^p015$ for all the other images.

The data were analysed using routines available at the Goddard Space Flight Center Regional Data Analysis Facility. Because the spectra are underexposed, smoothing beyond the optimal 3-point standard (which matches detector and spectrograph resolution) was required. This is a delicate procedure, as excessive smoothing can not only obscure important features but also introduce spurious ones. We performed a

number of comparison tests with a running boxcar filter, using the reseaux and the profiles of the sharp interstellar C IV lines as fiducial indicators in this connection. Easily perceptible changes in profile slope are produced by smoothing to more than 10 points; serious loss of information begins to occur with 20-point smoothing. We employ either 5- or 10-point smoothing, depending upon the S/N of the original image. Those archival spectra which were rejected because of inadequate S/N were found to require smoothing to 20 or more points before they could be intercompared.

In the cases of the strongest lines, N V $\lambda\lambda$1239,43 and C IV $\lambda\lambda$1548,51, improper interorder subtraction yields negative flux values at the bottoms of the saturated absorption troughs. The equivalent widths for these lines were computed by setting all negative fluxes to zero. The unsaturated He II λ1640 and N IV λ1718 absorption lines were free of this defect.

All the lines discussed below exhibit important periodic changes in line structure, especially near the cross-over point between the emission and absorption components of their P Cygni profiles. In many cases the line profile slope is greatest at precisely this cross-over point. These facts make it difficult to define the appropriate continuum level which separates the absorption and emission components, especially in relatively noisy spectra. The local pseudo-continuum outside the line is much more easily defined, whereby the wavelength interval for the total equivalent width (emission + absorption) can be dependably selected. Accordingly we quote only latter quantity; any interpretation of these data which depends upon the detailed parsing of the P Cygni structure is far less certain.

Finally, we infer the terminal velocity from the wavelength at which the extrapolated profile merges with the local pseudo-continuum. Careful tests of sample profiles subjected to different degrees of smoothing confirmed that negligible error in the measured terminal velocity is introduced by the smoothing procedure unless the width of the smoothing filter significantly exceeds that used in our reductions.

III. Results

Our analysis is based upon the variation of the four strongest P Cygni lines with orbital phase. The λ1640 and λ1718 lines, because they arise from highly excited states, are more sensitive indicators of wind structure within the binary orbit than are the resonance lines. The monotonic increase of SWP camera sensitivity with $\lambda \geq 1500\AA$ multiplies this advantage. Conversely, the resonance lines ($\lambda\lambda$1239,43 and $\lambda\lambda$1548,51) probe the velocity structure at large radii. The measured equivalent widths for the principal lines discussed in this section are listed in Table 3.

a. He II λ1640

The emission line always dominates this profile, whereby the total equivalent width is negative. The absorption is strongest at primary eclipse, weak at secondary eclipse and completely absent at phase 0.60. The single wave variation of W_{1640} with orbital phase is shown in Figure 1.

Near primary eclipse the emission profile is rounded, symmetric and red-shifted from the rest wavelength in the WR frame. The saturated absorption profile is also rounded, mirroring the emission profile shape. Figure 2 shows the contrast between the profile at primary eclipse and that at $\Phi = 0.^{p}60$.

Figure 3 shows gallery of line profiles which span the half of the orbit centered on secondary eclipse. Near quadratures, the emission profile strengthens slightly, developing an overall triangular shape peaked at the WR velocity with a steepened blue edge. The absorption profile also becomes triangular, giving a sawtooth appearance to the P Cygni line. Near secondary eclipse, the emission profile becomes slightly broader,

distinctly plateau-shaped with the steep blue edge characteristic of the quadrature profiles, and symmetric with respect to the WR velocity. These variations of the emission line profile do not extend to the high velocity red tail. Longward of approximately λ1645, the emission profile is invariant with orbital phase.

The terminal velocity inferred from the absorption line is clearly variable on time scales ranging between hours and days. There is no evidence for coherent variation with orbital phase, however. The terminal velocities, transformed to the binary center of mass frame (γ(O6) = 10 km s^{-1}), are shown in Table 4 and plotted against orbital phase in Figure 4.

b. N IV λ1718

A prominent absorption component, visible at most phases on the P Cygni line, reaches its maximum at primary eclipse and is weakest near secondary eclipse. The emission component is strongest near quadratures, when the absorption is also strong. This alternation between absorption- and emission-dominated profiles contrasts sharply with the character of the He II line, which is always strongly dominated by emission. The total equivalent width of λ1718, however, varies in phase with that of He II (see Table 3 and Figure 5).

The N IV emission feature near primary eclipse is round-topped on some orbits, flat-topped on others, but always centered significantly redward of the WR velocity. When the emission is weakest, the absorption sometimes extends redward of the WR velocity. The most important changes in the profile occur near secondary minimum, when the absorption component weakens, completely disappearing at $\Phi = 0.^{p}52$. The emission component also weakens beginning at $\Phi = 0.^{p}46$, but recovers by $\Phi = 0.^{p}76$. The occurrence of this almost pure emission profile is thus not phase-symmetric about secondary eclipse.

Near first quadrature (SWP 24731; $\Phi = 0.^{p}37$), the emission and absorption profiles are both triangular. The asymmetric emission is peaked at the WR velocity, shaded to the red and with a steep blue edge. Near third quadrature, the emission profile differs only in that it is shifted redward and truncated, forming a plateau-shaped profile.

The terminal velocity (see Table 4 and Figure 4) is generally consistent with that of He II, approximately constant on short timescales at about 2100 km s^{-1}. The absorption profile is generally asymmetric, displaying the steepest blue edge at the quadratures. When strongest the absorption is nearly saturated. An extensive gallery of λ1718 line profiles was presented in a preliminary report of these observations (Brown and Shore 1986). In Figure 6 we show the consistency of the profiles near primary minimum and the contrasting secondary eclipse profile.

c. C IV $\lambda\lambda$1548,51

The total equivalent width of this line is almost always approximately zero (equal fluxes in emission and absorption), suggestive of formation by scattering of light from a small core embedded in an optically thick primarily scattering medium. The deepest absorption is seen during primary eclipse.

The profile variations are not striking at most phases, so that, as noted by ECK, the low dispersion spectra supply little information. The emission profile varies between two relatively stable shapes. Between phases $0.^{p}37$ and $0.^{p}60$, the emission is skewed slightly to the blue. A steep blue emission edge is joined to a correspondingly steep red edge of the absoption profile. Between $0.^{p}92$ and $0.^{p}10$, the emission profile is shallower and more symmetrical, blending into the absorption line with a relatively shallow slope. Figure 7 displays the constancy of the profile through primary eclipse.

The transition between these forms occurs in a phase interval of approximately $0.^p1$ near third quadrature; the phase gap at first quadrature prevents us from observing the opposite transition. Except at those phases near secondary eclipse when the absorption to emission transition is very steep, the absorption and emission components join at $1548 \pm 1\AA$ in the WR frame.

The equivalent width varies by ± 4 Å (see Figure 8). The mean terminal velocity is 2620 ± 420 km s^{-1} (3.3σ variation). The most dramatic changes occur in the blue absorption wing near secondary eclipse. A high velocity blue-shaded tail develops at this phase, reaching a terminal velocity of 3800 km s^{-1}. The feature is present at phase $0.^p44$ and has disappeared by phase $0.^p76$. Figure 9 shows the phase variation of the terminal velocity, while a gallery of line profiles spanning secondary eclipse is shown in Figure 10.

The development of the high velocity tail is accompanied by a change in the strength of the emission feature, which becomes slightly broader and shallower. While this last effect may be real, it is more likely due to diminished low velocity absorption, as the redward edge of the blue-shifted absorption component is steepest at this phase. While the profile remains saturated at all phases, the total equivalent width of the line becomes most strongly negative (emission dominating) at this phase rather than at primary eclipse.

d. N V λλ1239,43 Å

Because this doublet is badly blended with Lyα and falls in a noisy portion of the spectrum, the variations can be only roughly characterized. The structure of the line is typical for the resonance line of a WR star. The profile is always saturated but the structure of the absorption trough, unlike that of C IV, is entirely dominated by

noise and blends. The terminal velocity appears to be comparable to that exhibited by the C IV line, and the same high velocity tail seems to develop at phase $0.^p60$. The poor S/N of the data in this part of the camera, however, renders these judgments uncertain.

III. Discussion

The C IV and N V resonance lines certainly contain contributions from both components, but the He II and N IV lines appear in the spectra of O6 stars as unsaturated absorption lines with no hint of P Cygni emission (Walborn *et al.*, 1986). Therefore, all the emission and much of the absorption observed in these lines must arise in the WR wind. We therefore discuss the interpretation of the resonance and non-resonance lines separately.

a. He II and N IV

Assuming the CEK solution for the O-star and WR core radii, the well-determined orbital inclination implies that only slightly more than half of the WR core is eclipsed at secondary minimum. Accordingly, the more than two-fold weakening of the λ1718 and λ1640 absorption at that phase implies that either, (a) the CEK value of the WR core radius is too large, so that the WR core is actually more substantially eclipsed or, (b) these absorption lines are formed almost entirely by absorption and scattering of the O-star (rather than the WR) continuum in the WR wind. We adopt the CEK photometric solution and hypothesis (b), arriving at the following deductions.

1. The presence of the absorption features at quadrature implies that the WR wind envelopes the entire system. ECK reached a similar conclusion on the basis of their continuum light curves for $\lambda < 1500\AA$.

2. The disappearance of the λ1718 and λ1640 absorption near secondary eclipse implies a dramatically lower density of the WR wind in the line of sight at those phases. ECK noted the weakening of the absorption features in their low dispersion spectra and interpreted it as a result of a binary reflection effect. The reflection (presumably resonant backscattering) of O-star continuum light by the (approaching) near side of the WR wind was assumed responsible for filling in the absorption line and for augmenting the emission profile, thus accounting for the observed hump in their narrow band light curves. Our high resolution spectra are clearly inconsistent with this suggestion. It is well known that the Doppler shift imposed by a "moving mirror" is twice the velocity of the mirror. CEK determined that the wind emerges from the WR core at 500 km s^{-1} and reaches terminal velocity (≈2000 km s^{-1} in the He II and N IV lines) at roughly half the separation of the binary components. Resonant backscattering would thus produce a broad enhancement of the continuum, extending between 1000 km s^{-1} and 4000 km s^{-1} ($4 - 20\AA$) from the rest wavelength in the WR frame. The gallery of λ1640 spectra in Figure 3 show no hint of such a feature. It is difficult to imagine a scattering geometry which would so convincingly mimic a reduced column density in the line of sight.

3. The fact that He II and N IV emission is strongest at quadrature implies that the strongest emitting/scattering region is on the side of the WR wind facing the O-star. The weakness of N IV emission near primary eclipse supports this inference.

4. The remarkable constancy of the He II emission profile through primary eclipse confutes the suggestion of a material stream from the WR toward the O-star, as such a stream would presumably produce a recognizable redshifted absorption at these phases. The eight profiles which fall in the interval $0.^p89$ and $0.^p09$ are identical within the photometric uncertainty. Redward of 500 km s^{-1} from the WR velocity

(roughly the velocity which CEK attribute to the WR wind at the photosphere) even the profiles at $0.^p76$ and $0.^p00$ are identical.

b. C IV

Notwithstanding the uncertainty in identifying the cross-over point between the emission and absorption components of the line profile, it is clear that the red absorption edge is never less than 200 km s^{-1} from the WR velocity at any phase. The absence of low velocity absorption suggests that the WR wind is optically thick and supersonic even at the photosphere, as inferred by CEK from their IUE spectrophotometry.

The C IV profiles at third quadrature and at $\phi = 0.^p37$ differ very little in shape; they are almost identical except for a relative velocity shift of approximately 400 km s^{-1}, somewhat less than the relative WR velocity difference between those two phases. It appears that the contribution of the O-star to the P Cygni profile at these phases must be slight, whereby the profile variations must be interpreted in terms of a non-spherically symmetric wind structure.

The interval of orbital phase during which the high velocity tail develops in C IV and the absorption almost disappears from the λ1718 line is moderately well resolved in our data. It is evidently asymmetric about secondary eclipse ($0.^p44 \leq \Phi \leq 0.^p60$) and appears to be sharply bounded in phase: one edge occurs between $0.^p37$ and $0.^p44$, the other between $0.^p60$ and $0.^p76$. The absorption disappears from λ1640 not at secondary eclipse, but at $\Phi = 0.^p60$. These characteristics suggest a dynamical origin for the phenomenology.

c. Wind - Wind Interaction

The simplest explanation is that we are seeing a cavity trailing behind the O star: a shadow in the WR wind, produced by the interaction of the winds of the two

stars. If Walborn's (1974) luminosity classification (O6-8 III) is correct, the O-star likely possesses a more substantial wind than typical for a main sequence star of its mass. A standing shock would accordingly be expected at the interface between the two winds. We interpret the high velocity tail of the C IV resonance line as evidence of an oblique shock at the boundary of the interaction region and the absence of the He II and N IV absorption as evidence that the O star effectively shadows the WR wind. When the cavity crosses our line of sight, we see the lower density O-star wind. In the resonance lines, we see the asymptotic material velocity in the interaction region projected onto the line of sight. The emission is, as usual, interpreted as the result of scattering the O-star light off the WR wind.

The relative orbital velocity of the O-star with respect to the WR wind yields an aberration angle of approximately $0.^{p}03$ between the line of centers and the axis of the "wind shadow" cavity. This value is consistent with the observed phase offset of the spectral indicators with respect to secondary eclipse. The opening angle of the wind cavity appears to be approximately 60° so that the line of sight is parallel to the asymptotic conical surface of the interaction region at only two phases: shortly before and after secondary eclipse. The resonance lines should exhibit the highest velocity blue-shifted absorption at these phases. In the interval $0.^{p}45 - 0.^{p}60$, the "terminal" velocity observed in these lines will be reduced by $cos|(90° - i) - 30°| \approx 0.9$. Figures 11 and 12 show a pair of cartoons which represent the geometry suggested by these considerations. Further details of the model are discussed in the next section.

Underhill and Fahey (1987, hereafter UF) have proposed a very different model for V444 Cygni on the basis of a diverse set of high resolution IUE spectra, many obtained during the higher noise US2 shift. An important element of their critique of the CEK photometric solution was noted above: the imputed presence of a phase-

dependent "third light" in the system. The ultraviolet continuum fluxes which UF derive from high resolution spectra are certainly less affected by unresolved weak emission lines than are the CEK fluxes. The high resolution calibration, however is far less secure than that of the low resolution spectra used by CEK. The high resolution photometric calibration is poorest at the short wavelength end of the SWP camera, where crowding of the echelle orders complicates the background subtraction. The fluxes derived from even optimally exposed spectra are dependable to no better than 10%. For non-optimal images, other difficulties diminish the photometric accuracy. Oliversen (1984) found that near 1300Å, where UF find the greatest divergence from the CEK light curve, linearity errors of 10 – 20% are not uncommon in trailed low resolution spectra if, like the spectra of UF, they are underexposed and degraded by high particle background. High resolution spectra may be expected to suffer (at least) comparable linearity errors.

We have supplemented our US1 observations with those of the UF spectra which have roughly comparable S/N. Yet, we find no evidence in the resulting set of λ1640 or λ1718 profiles for the compact plasma tubes which they suggest link the two stars. For example, the peaks of the λ1640 profiles in Figure 3 track the WR star velocity.

One possible origin of the features which they discuss is the smoothing procedure which they employ. It is important to note that a 51-point smoothing is not equivalent to binning with 10Å resolution because the smoothing algorithm performs a running average centered on *each* pixel. In order to improve S/N at the expense of resolution, it is necessary to average the data in *non-overlapping* wavelength bins. This procedure avoids the generation of correlated errors in independent pixels.

IV. Toward a Model for V444 Cygni

Interacting winds have been received relatively little attention in the literature.

Cherepashchuk (1976) and Prilutskii and Usov (1976) have presented qualitative discussions applicable to WR binaries. Chapman (1981), Huang and Weigert (1982) and Girard and Willson (1987) have undertaken more extensive analysis, but for systems which bear little resemblence to V444 Cygni.

For simplicity, we assume that the winds of both stars have reached terminal velocity prior to collision. The most recent models of Pauldrach *et al.* (1986) suggest that this is the case for the WR wind in V444 Cygni, but it may be only approximately true for the O-star wind. The location of the stagnation point is determined by the equality of the wind dynamical pressures. Taking $\alpha = (\dot{M}_2 v_2 / \dot{M}_1 v_1)^{1/2}$ gives $x = (\frac{\alpha}{1+\alpha})$ for the position of the stagnation point with respect to the O-star in terms of the binary separation. Since the velocities of both winds are very high, we neglect the effects of orbital motion except for a slight aberration from the line of centers. There is no evidence that the WR wind is directly impinging on the surface of the O star, so that α must be sufficiently small that the stagnation point is well separated from its photosphere. The opening (full cone) angle of the shock relative to the WR star is about $\theta = 40°$ so that an approximate solution gives $x \approx 0.3$.

This places the stagnation point close to the center of mass of the system and serves as a constraint on the mass loss rate from the O star. The derived value is $\alpha = 0.3 - 0.5$. Assuming that the wind velocities are approximately equal, $\dot{M}_O \approx (1-3) \times 10^{-6} M_\odot yr^{-1}$. This value is far closer to that of an evolved than main sequence O star, consistent with the spectroscopic classification of Walborn (1974). We also note that none of the ultraviolet spectral features conflicts with Walborn's luminosity class assignment.

IV. Conclusion

We interpret the abrupt increase near secondary eclipse in the λ1550 terminal

velocity and simultaneous decrease in the material density indicated by λ1640 and λ1718 absorption as evidence for a shock dominated wind-wind interaction between the binary components of V444 Cygni. Our high resolution IUE spectra provide no evidence for the existence of material streaming between the two stars, as suggested by Kuhi (1968a) or of magnetically configured plasma plumes and tubes, as suggested by Underhill and Fahey (1987).

Because the momenta of the two winds are large and the hydrodynamics of their collision is complex, only a preliminary outline of a model is currently possible. A qualitative prediction is, however, implied. Of the four other currently known (WR + O) eclipsing binaries, only CQ Cep should exhibit similar phenomenology in IUE spectra. The separation of the components of CV Ser is likely too large in comparison with the wind momenta for a similar structure to be produced. GP Cep is a relatively compact quadruple system in which the winds of all four components may play a role. CX Cep is much too faint for IUE observations. Stickland *et al.* (1984) noted an apparent depletion of He II and N IV at primary eclipse, when the leeward side of the presumed O-star companion crosses the line of sight. We predict that high resolution observations will reveal an abrupt increase in the λ1550 terminal velocity at phases near the eclipse.

A second implication of the proposed model is that detectable linear polarization would be expected in the UV emission lines because of the presumed importance of resonance scattering in their formation. The optical thickness of the lines contrasts with the optically thin continuum, rendering a quantitative prediction beyond the scope of this paper.

The importance of V444 Cygni as a unique astronomical laboratory for the study of steady state thermodynamics and hydrodynamics in colliding stellar winds amply

justifies the theoretical and observational effort which will be required to refine the model and test its predictions.

Acknowledgements

We wish to thank Drs. N. Bochkarev, C. Catala, J. Castor, J. Eaton, R. Fahey, R. Hjellming, G. Koenigsberger, Y. Kondo, J. Sahade, G. Sonneborn, A. Torres,and N. Walborn for enjoyable discussions about Wolf-Rayet systems in general and our study in particular. SNS warmly thanks Dr. P. Encrenaz and Dr. F. Praderie for their invitation to the Observatoire de Meudon during Summer 1986 when some of the preliminary work in this study was carried out. This work is supported by NASA grant NAG 5-357 to the University of Washington.

REFERENCES

Abbott, D.C., Bieging, J.H., Churchwell, E., Torres, A. 1986, *Ap. J.*, **303**, 239.

Bieging, J.H., Abbott, D.C., and Churchwell, E.B. 1982, *Ap.J.*, **263**, 207.

Bisiacchi, G.F., Firmani, C., and de Lara, E., 1982, in *Wolf- Rayet Stars: Observations, Physics and Evolution*, IAU Symposium No. 99, ed. de Loore, C. and Willis, A. (Dordrecht; Reidel), p. 283

Brown, D. and Shore, S. 1986, in New Insights in Astrophysics, Proc. Joint NASA/ESA/SERC Conf., ESA SP-263, p. 353.

Castor, J., Abbott, D. and Klein, R. 1975, *Ap.J.*, **195**, 157.

Castor, J. and Lamers, H. 1979, *Ap.J.Suppl.*, **39**, 481 .

Castor, J., Lutz, J. and Seaton, M. 1981, *MNRAS*, **194**, 547.

Chapman, C.R. 1981, *Ap.J.*, **248**, 1043

Cherepashachuk, A.M. 1976, *Sov.Astr.Lett.*, **2**, 138.

———————— 1982, *Astr.Sp.Sci.*, **86**, 299.

Cherepashchuk, A. and Khaliullin, Kh. 1973, *Sov.Astr.-AJ*, **17**, 330.

Cherepashchuk, A., Eaton, J., and Khaliullin, Kh. 1984, *Ap.J.*, **281**, 774 (CEK).

Eaton, J., Cherepashchuk, A. and Khaliullin, Kh. 1985, *Ap.J.*, **297**, 266 (ECK).

Girard, T. and Willson, L. 1987, *preprint.*

Hamman, W-R. 1985, *Astr. Ap.*, **145**, 443.

Hiltner, W.A. 1949, *Ap.J.*, **110**, 95.

Huang, R. and Weigert, A. 1982, *Astr. Ap.*, **112**, 281.

Keeping, E.S. 1947, *Publ. Dom. Ap. Obs.*, **7**, 349.

Khalliullin, Kh. 1974, Sov. Astr.-AJ, **18**, 229.

Khalliullin, Kh. and Cherepashchuk, A. 1976, *Sov. Astr.-AJ*, **20**, 186.

Koenigsberger, G. 1984, *Rev.Ap.Mex.*, **9**, 159.

Koenigsberger, G. and Auer, L. 1985, *Ap.J.*, **297**, 255.

Kopal, Z. 1944, *Ap.J.*, **100**, 204.

Kopal, Z. and Shapley, M. 1946, *Ap.J.*, **104**, 160.

Kornilov, V. and Cherepashchuk, A. 1979, *Sov. Astr. Lett.*, **5**, 214.

Kron, G. and Gordon, K. 1943, *Ap.J.*, **97**, 311.

— 1950, *Ap.J.*, **111**, 454.

Kuhi, L. 1968a, *Ap.J.*, **152**, 89.

—— 1968b, in *Wolf-Rayet Stars*, ed. Gebbie, K. and Thomas, R., Nat. Bur. Stds. Spec. Publ. 307, (Washington, D.C.: U.S. Gov. Print. Off.)

Munch, G. 1950, *Ap.J.*, **112**, 266.

Oliversen, N. 1984, NASA IUE Newsletter No. 24, p. 27.

Pauldrach, A., Puls, J., Hummer, D., and Kudritzki, R., 1985, *Astr. Ap.*, **148**, L1.

Prilutskii, O. and Usov, V. 1976, *Sov. Astr.-AJ*, **20**, 2.

Rudy, R. and Kemp, J. 1978, *Ap.J.*, **221**, 200.

Russell, H.N. 1944, *Ap.J.*, **100**, 213.

Sahade, J. 1958, *Mem. Soc. Roy. Sci. Liege*, **20**, 46.

Stickland, D., Bromage, G., Budding, E., Burton, W., Howarth, I., Jameson, R., Sherrington, M., and Willis, A., 1984, *Astr. Ap.*, **134**, 45.

Underhill, A. 1966, *The Early Type Stars* (Dordrecht:Reidel)

———— 1983a, *Ap.J.*, **265**, 933.

———— 1983b, *Ap.J.*, **266**, 718.

———— 1984a, *Ap.J.*, **276**, 583.

———— 1984b, *Ap.J.*, **287**, 874.

Underhill, A. and Fahey, R. 1987, *Ap.J.*, **313**, 358 (UF).

Walborn, N. 1974, *Ap.J.*, **189**, 269.

Walborn, N., Nichols-Bohlin, J. and Panek, R. 1985, *International Ultraviolet Explorer Atlas of O-Type Spectra*, NASA Ref. Publ. 1155

Wilson, O.C. 1940, *Ap.J.*, **91**, 379.

———— 1942, *Ap.J.*, **95**, 402.

Wright, A. and Barlow, M. 1975, *M.N.R.A.S.*, **170**, 41.

Table 1. Journal of New Observations

SWP	Exposure (minutes)	JD - 2,440,000	Φ
25962	192	6202.884	0.098
25990	245	6207.023	0.080
25994	200	6208.889	0.523
26000	192	6209.891	0.761
26007	200	6210.886	0.997
26008	205	6211.248	0.036
26030	200	6214.890	0.948
26031	205	6215.051	0.986
26041	202	6217.050	0.461
26065	200	6218.812	0.879
26066	200	6218.968	0.916

Table 2. Journal of Archival Spectra

SWP	Exposure (minutes)	JD - 2,440,000	Φ
14553[a]	90	4811.396	0.773
24731[b]	170	6056.580	0.366
24734[b]	180	6057.578	0.603
24740[b]	195	6058.587	0.843
24745[b]	200	6059.583	0.079
25904[c]	200	6195.887	0.437
25905[c]	205	6196.049	0.475

Notes:

[a] VILSPA image.

[b] US2 image.

[c] US1 image.

Table 3. Equivalent Widths (Å)

SWP	Φ	N V 1240	C IV 1550	He II 1640	N IV 1718
14553	0.773	2.8	-2.1	-23.9	-2.4
24731	0.366	0.48	-0.8	-18.9	-3.7
24734	0.603	-3.0	2.8	-25.4	-5.8
24740	0.843	2.7	-1.8	-20.2	0.8
24745	0.079	3.0	0.6	-15.7	3.1
25904	0.437	1.2	-0.5	-19.2	-3.3
25905	0.475	4.2	1.1	-17.1	-3.5
25962	0.098	1.3	1.8	-16.1	2.1
25990	0.080	2.8	3.1	-15.3	3.3
25994	0.523	5.3	3.5	-20.7	-4.4
26000	0.761	4.3	-3.3	-21.3	-3.2
26007	0.997	-3.7	0.7	-19.3	1.7
26008	0.036	-12.2:	-1.0	-14.3	3.0
26030	0.948	-21.1:	2.6	-12.8	4.7
26031	0.986	-6.8	0.6	-15.6	1.8
26041	0.461	1.7	-1.1	-21.1	-2.2
26065	0.879	-3.7	-0.0	-13.9	1.0
26066	0.916	-6.5	0.6	-13.1	4.0

Table 4. Terminal Velocities (km s^{-1})

SWP	Φ	$v_r(O6)$[a]	$v_r(WR)$[a]	$v_t(1550)$	$v_t(1640)$	$v_t(1718)$
14553	0.773	110	-292	-2380	-2040	-2300
24731	0.366	-90	238	-2340	-2050	-1590
24734	0.603	72	-174	-3480	-1170	-1810
24740	0.843	100	-244	-2270	-1890	-2570
24745	0.079	-58	155	-2100	-1750	-2520
25904	0.437	-46	128	-3230	-1780	-1930
25905	0.475	-19	58	-3050	-2330	-1640
25962	0.098	-69	186	-2180	-2400	-2100
25990	0.080	-58	157	-2180	-2170	-1820
25994	0.523	17	-34	-3370	-1980	-2180
26000	0.761	120	-294	-2670	-1820	-1860
26007	0.997	2	4	-2410	-1910	-1910
26008	0.036	-27	78	-2310	-1880	-1980
26030	0.948	38	-88	-3290	-2760	-2560
26031	0.986	10	-17	-2290	-2440	-2530
26041	0.461	-29	84	-3810	-1980	-2030
26065	0.879	83	-200	-2310	-2440	-2480
26066	0.916	60	-144	-2260	-2340	-2250

Note:

[a] Derived from Munch (1950).

DOUGLAS N. BROWN: Department of Astronomy FM-20, University of Washington, Seattle, WA 98195

STEVEN N. SHORE: Astrophysics Research Center, Department of Physics, New Mexico Institute of Mining and Technology, Socorro, NM 87801

FIGURE CAPTIONS

Figure 1. Orbital phase variation of He II λ1640 total equivalent width. The uncertainty in phase is less than the size of the plotting symbols.

Figure 2. Comparison of four He II λ1640 line profiles near primary eclipse with that at 0.60 (SWP 24734). The eclipse profiles are from SWP 26007, 26008, 26030 and 26031. Note the complete absence of absorption at 0.60.

Figure 3. Gallery of He II λ1640 line profiles spanning secondary eclipse. Phase advances from the bottom (0.37) to the top (0.84) of the figure. Note that the absorption component is almost absent between 0.44 and 0.76.

Figure 4. Orbital phase variation of terminal velocities measured in He II λ1640 (triangles) and N IV λ1718 (dots). The uncertainty in phase is less than the size of the plotting symbols.

Figure 5. Orbital phase variation of N IV λ1718 total equivalent width.

Figure 6. (a) Overplot of N IV λ1718 line profiles near primary eclipse. The spectra are taken from the same images as in Figure 2.

(b) Comparison of N IV λ1718 line profile at secondary eclipse (SWP 25994, 0.52) and just before onset of primary eclipse (SWP 26065, 0.88). Compare with Figure 3; note that the absorption component of λ1718 disappears at earlier phase than does that of λ1640.

Figure 7. Overplot of C IV λ1550 line profiles near primary eclipse. The spectra are taken from the same images as in Figure 2.

Figure 8. Orbital phase variation of C IV λ1550 total equivalent width.

Figure 9. Orbital phase variation of C IV λ1550 terminal velocity. Note that the increased wind velocity coincides in phase with the weakening of He II and N IV absorption.

Figure 10. Gallery of C IVλ1550 line profiles spanning secondary eclipse. Phase advances from the bottom (0.37) to the top (0.84) of the figure. Note the presence of enhanced blueshifted absoption between 0.44 (SWP 25904) and 0.60 (SWP 26000).

Figure 11. Cartoon of the proposed wind - wind interaction in V444 Cygni. Top view along the normal to the orbital plane. The SWP image numbers of spectra discussed in the text are indicated at the corresponding orbital phases on the reference circle.

Figure 12. Cartoon side views of the V444 Cygni system at secondary eclipse showing the proposed structure of the wind - wind interaction. Direction of observer is to the right.

(a) View along the line of nodes.
(b) View along the line of sight.

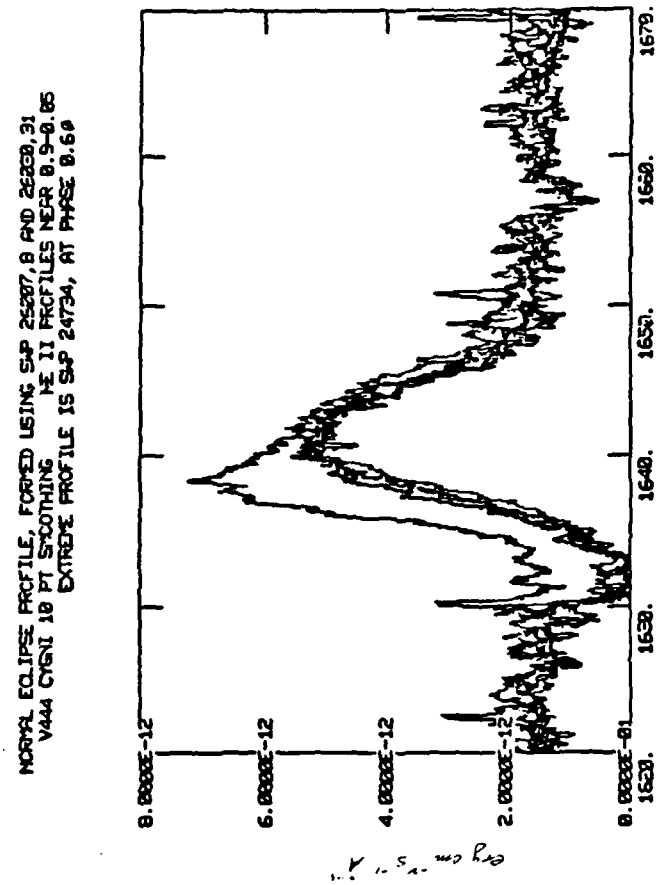

FIGURE 2

ORIGINAL PAGE IS
OF POOR QUALITY

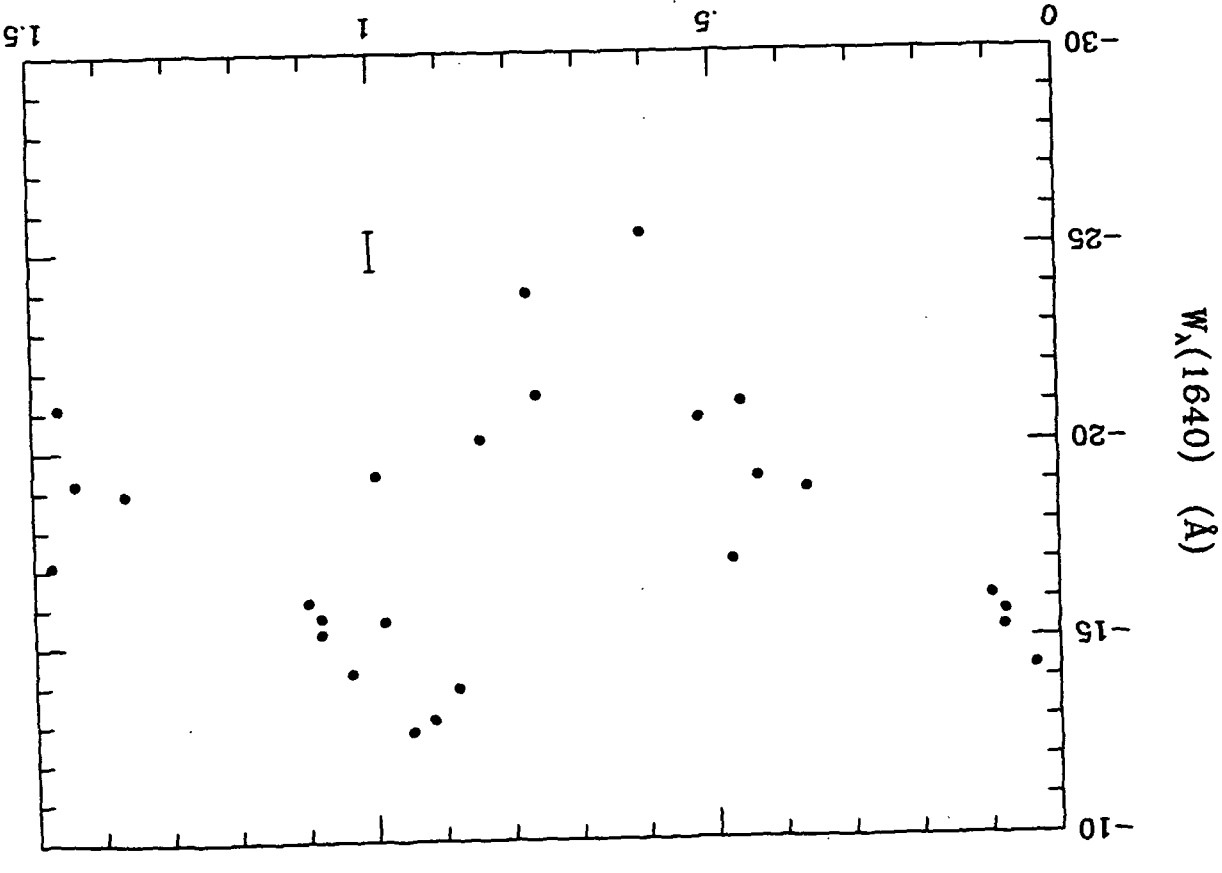

FIGURE 1

FROM BOTTOM TO TOP SWP 25994,24734,25000,24740
5 PT SMOOTHING V444 CYG HE II

FIGURE 3

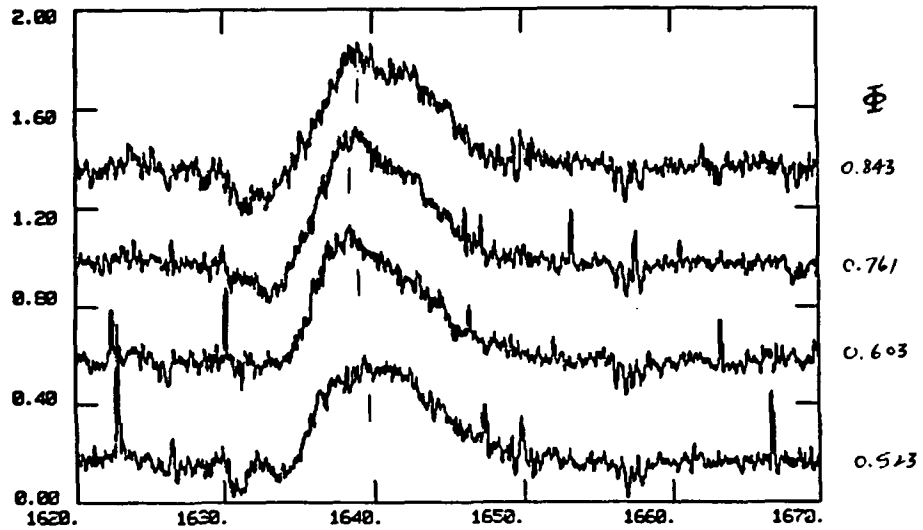

SWP 24731,25984,25041,25985 FROM BOTTOM TO TOP
5 PT SMOOTHING V444 CYG HE II LINES

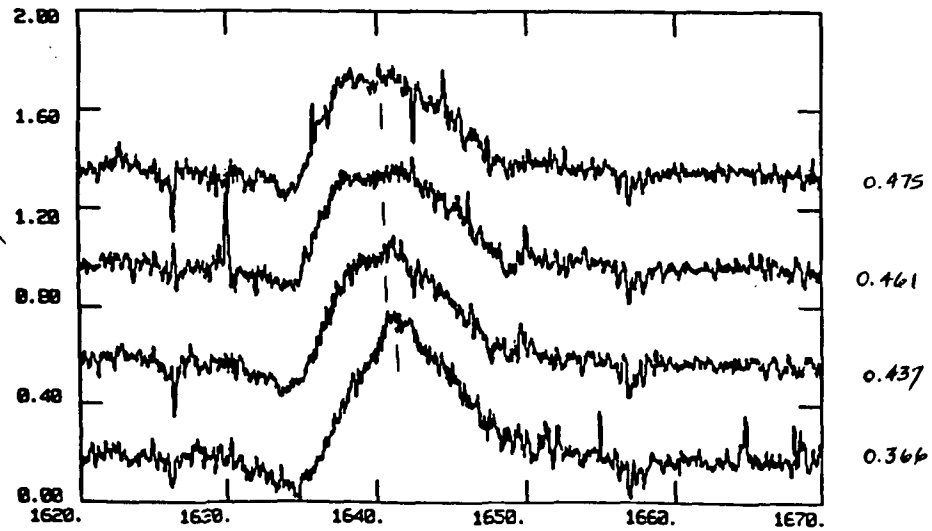

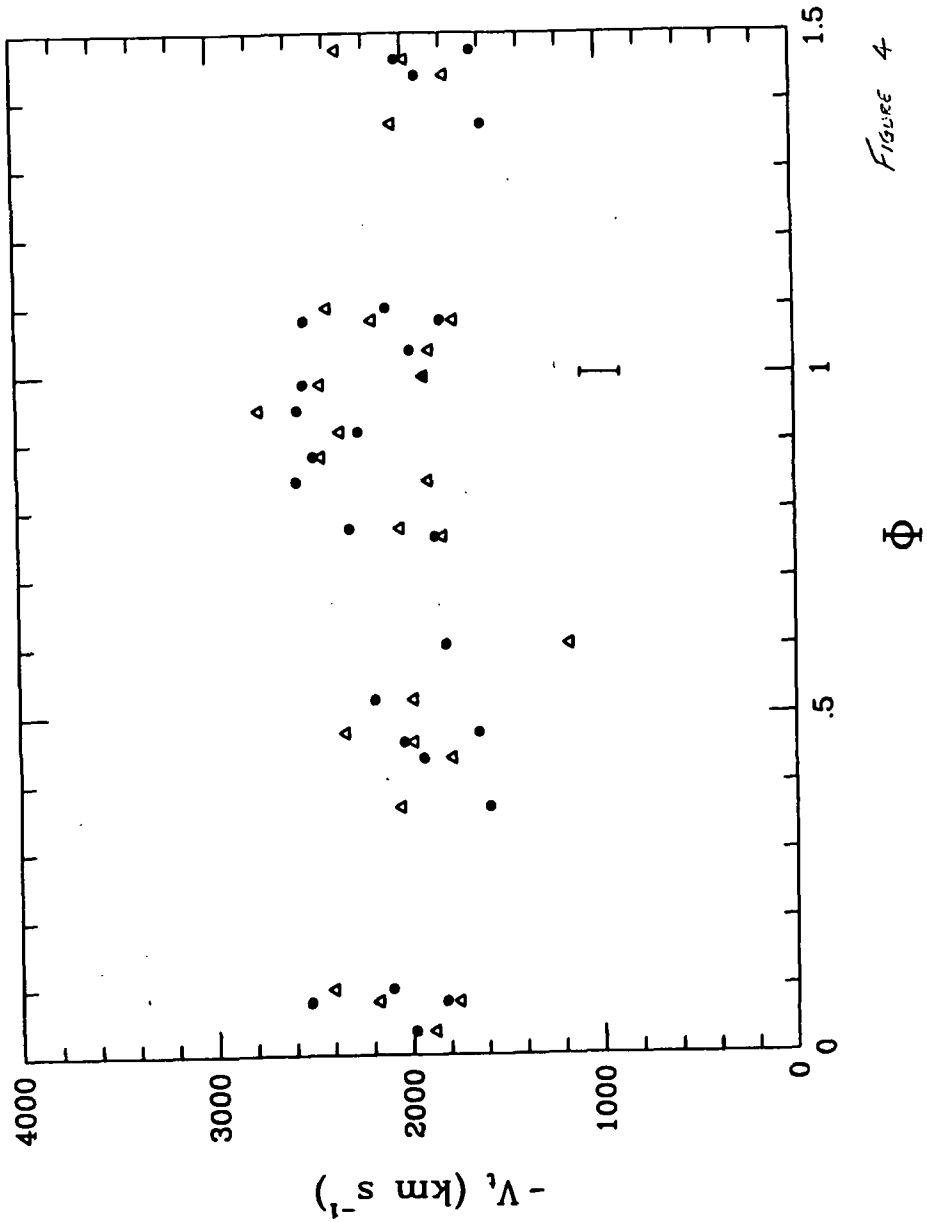

FIGURE 4

FIGURE 5

FIGURE 6

Figure 7

Figure 8

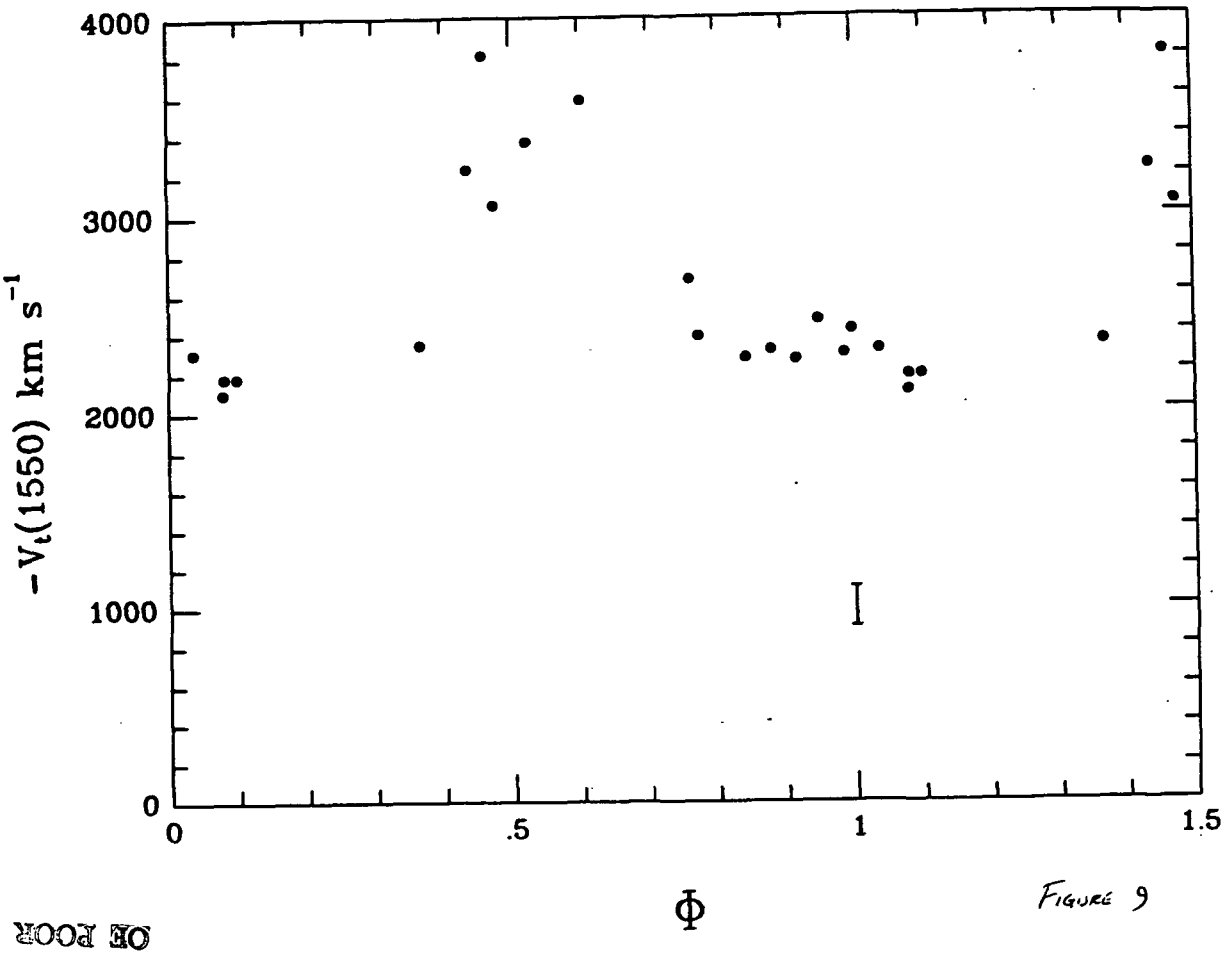

FIGURE 9

ORIGINAL PAGE IS
OF POOR QUALITY

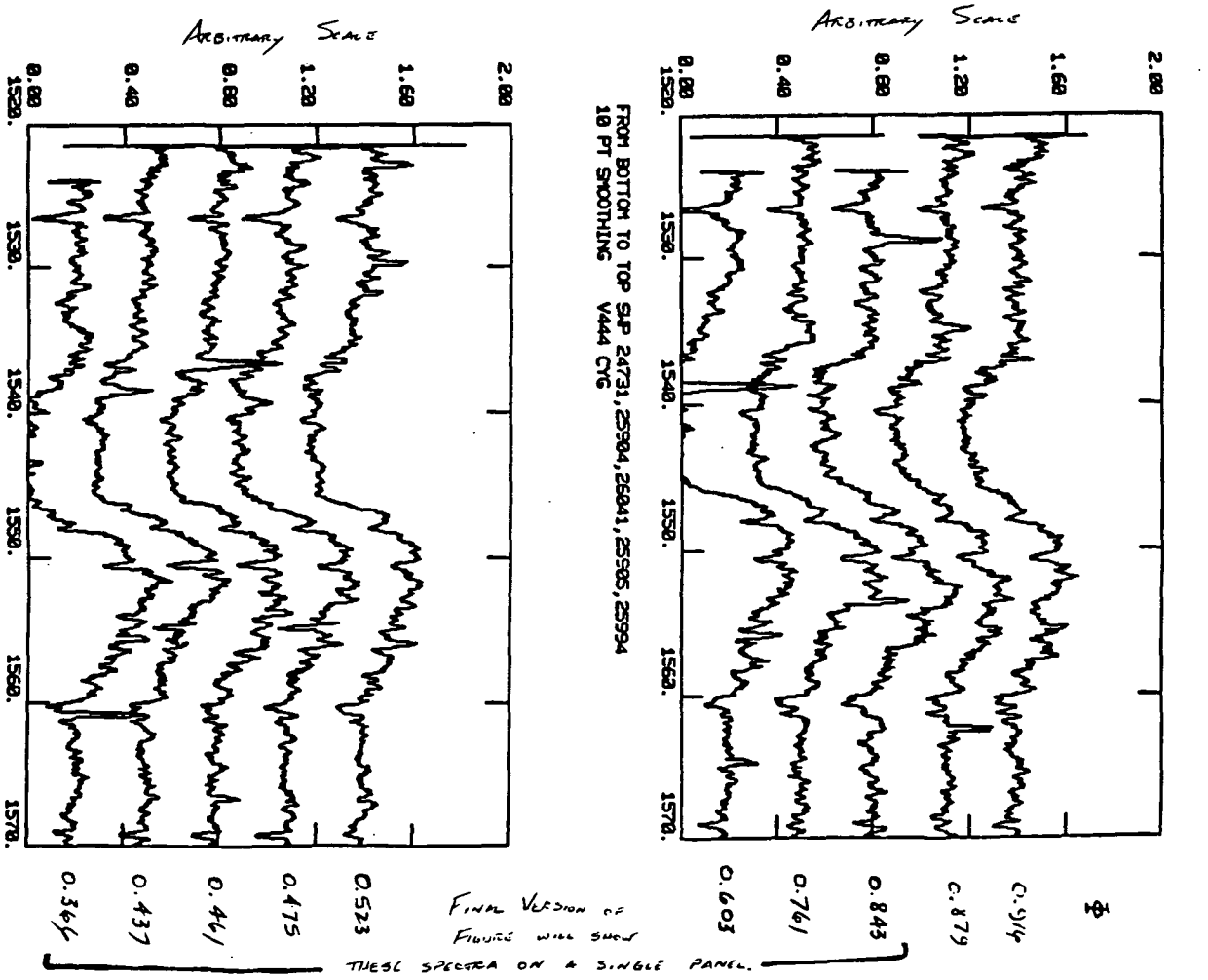

FIGURE 10

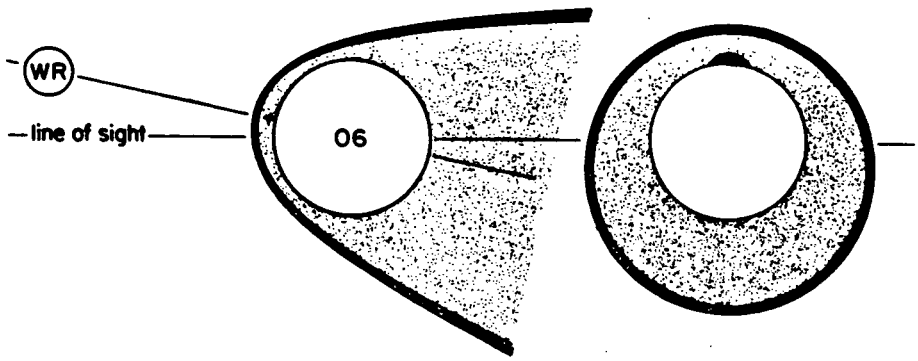

(a) (b)

FIGURE 12

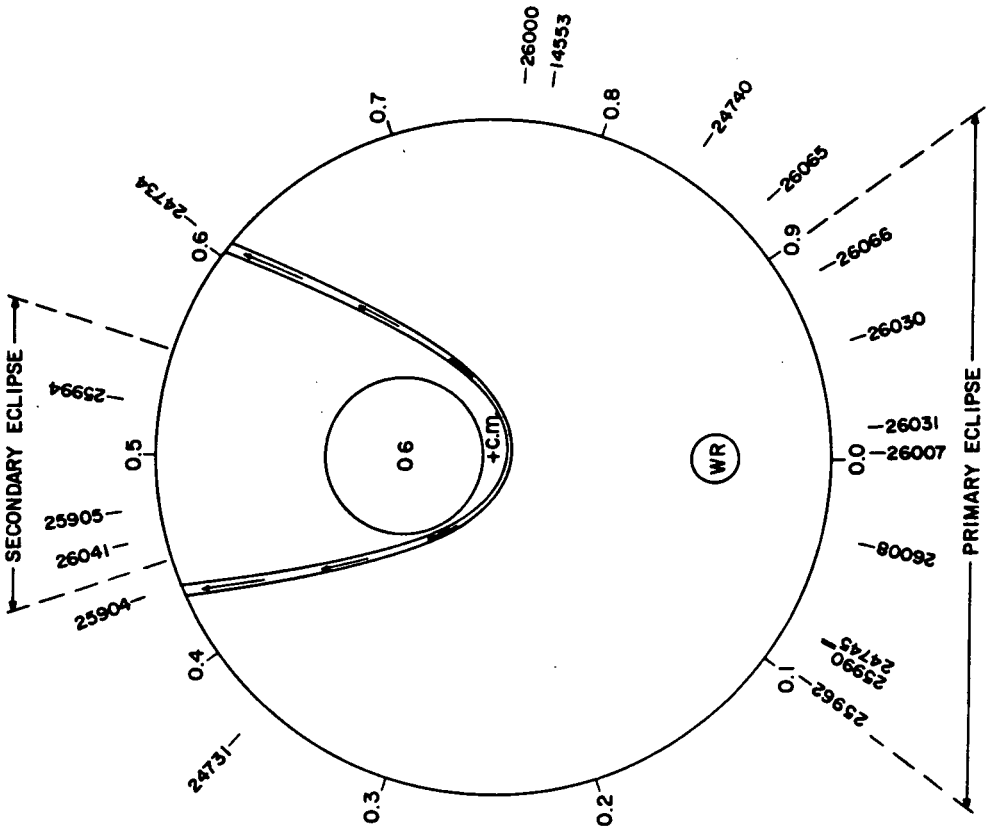

FIGURE 11